

Borehole-to-surface electrical resistivity monitoring of a salt water injection experiment

D. Bevc* and H. F. Morrison*

ABSTRACT

A field experiment was conducted at the University of California Richmond Field Station to demonstrate the sensitivity of borehole-to-surface resistivity measurements in groundwater investigations. A quantity of saline water was injected into a fresh water aquifer while the resistivity was monitored using a multichannel borehole-to-surface system. Two experiments were conducted using pole-pole and pole-dipole receiver electrode arrays. The data from the pole-pole experiment were superimposed to simulate a dipole-pole array and the data from the pole-dipole array were superimposed to simulate a dipole-dipole array. This superposition of the data was done to enhance the anomaly and facilitate interpretation.

A numerical modeling study was performed in conjunction with the field experiment in order to interpret the results. A three-dimensional modeling program was used to simulate the geological setting of the field experiment and the salt water injection. This modeling revealed that an asymmetric displacement of the salt water slug results in asymmetric current channeling which is observable as a 25 to 40 percent difference between preinjection and postinjection borehole-to-surface resistivity.

In addition to demonstrating the sensitivity of subsurface arrays, this experiment demonstrated that the measurement of bulk resistivity can identify a groundwater flow pattern not detected by hydrological measurements.

INTRODUCTION

The increase of activity in hydrogeology has led to the assessment of geophysical methods for mapping contaminant plumes and monitoring groundwater migration. Of all geophysical techniques, electrical methods have had the most widespread use in groundwater investigations because many contaminants decrease the pore water resistivity which reduces the bulk earth resistivity (Saunders and Stanford, 1984; Rodriquez, 1984). Surface resistivity surveys have been used successfully to delineate aquifers, locate fresh, brackish, and saline water-bearing zones (Van Overmeeren, 1989) and to determine the bulk groundwater velocity and hydraulic conductivity (White, 1988). Unfortunately surface methods do not work well for low resistivity contaminants and areas of conductive overburden if the zone of interest is too deep. Furthermore, the sensitivity of surface surveys is strongly influenced by the inhomogeneous near-surface layer (Asch and Morrison, 1989).

Many authors have used various numerical examples to demonstrate that subsurface features are more easily detected if some or all of the electrodes are placed in the subsurface (Daniels, 1977; Yang and Ward, 1985a, b; Beasley and Ward, 1986). Daniels (1983) used a borehole-to-surface resistivity array to define geoelectric inhomogeneities in a layered volcanic sequence. Le Masne and Poirmeur (1988) used a three-dimensional (3-D) integral equation program to interpret a borehole-to-surface survey and delineate pyritic conductors in granite. The same program was also used to interpret a cross-hole survey in a similar environment (Poirmeur and Vasseur, 1988).

This paper is concerned with similar geometries, but in more conductive terrain and with anomalies due to changes in pore fluid resistivity. Wilt et al., (1983) used the 3-D program developed by Dey and Morrison (1979) to model a geothermal reinjection process, and Wilt and Tsang (1985) later used the same program to simulate subsurface contaminant migration. They found that an order of magnitude

Manuscript received by the Editor April 30, 1990; revised manuscript received December 6, 1990.

*Engineering Geoscience, 414 Hearst Mining Building, University of California, Berkeley, CA 94720

©1991 Society of Exploration Geophysicists. All rights reserved.

increase in sensitivity can be achieved when the current source is placed downhole and within the electrolytic contaminant zone. This paper describes a borehole-to-surface electrical resistivity field experiment designed to confirm the numerical results by monitoring the injection of a salt water slug into a fresh water aquifer.

Two separate experiments were conducted at the University of California Richmond Field Station (RFS) using two different receiver electrode arrays. The first experiment utilized a pole-pole data acquisition configuration with transmitter electrodes on the surface and downhole. The second experiment utilized a pole-dipole arrangement with transmitter electrodes downhole. In both cases, the receiver electrodes were located on lines radiating from the injection well. The data were interpreted using a 3-D resistivity modeling program, and compared to hydrologic measurements taken during the injection.

EXPERIMENTAL SETTING

The experiments took place in February, 1988 and February, 1989 at the University of California Richmond Field Station, an industrial area adjacent to San Francisco Bay and about six miles northwest of the Berkeley Campus. The site was chosen for its accessibility, suitable geological conditions, and the availability of a supply of salt water for fluid injection. The well field is located in an open area 400 m north of San Francisco Bay.

Eight wells were drilled to depths ranging from 30 m to 40 m (Figure 1) through a deltaic sequence of unconsolidated clay and silt with intermittent lenses of sand and gravel. Analysis of the driller's logs shows that several of the clay horizons can be traced throughout the well field, but that many sand and gravel bodies are lenticular connecting three or four of the wells at most.

The field site was characterized by seismic, resistivity, electromagnetic, and borehole induction log surveys. For numerical modeling purposes, the data from these experiments are adequately interpreted by a four-layer model. The surface layer is 2 m thick and has a resistivity of $17 \Omega \cdot \text{m}$ when dry, and $5 \Omega \cdot \text{m}$ when saturated by rainwater. This is underlain by a thin layer with conductivity thickness product of about 0.5 S and an $11 \Omega \cdot \text{m}$ layer extending to a depth of 40 m and representing the interbedded sequence of deltaic deposits. The whole sequence lies on top of a $50 \Omega \cdot \text{m}$ half-space.

All the wells are cased with PVC. Two of the wells, INJ and EXT, are 6 inches in diameter and were designed for fluid injection and withdrawal experiments. These wells have steel sections for current injection at 20 m and 40 m and a metal screen segment at 30 m. The latter was chosen to allow injection and withdrawal of fluids in the sand and gravel aquifers that are at this depth. The metal electrode segments are connected by individual cables to the current transmitter on the surface. The remaining six holes (OBS1-OBS6) are 4-inch diameter wells drilled to depths ranging from 30–35 m. These wells are open at the bottom and designed for use in water level measurement and downhole water sampling.

Piezometric levels were measured in the wells at various dates. These measurements showed that under undisturbed

conditions, flow in the vertically confined aquifer was from north to south and the average gradient of the piezometric level was about 0.003. Several pumping tests were carried out in different wells to calculate hydrologic properties of the aquifer. Values of drawdown from observation wells 1, 4, 5, and 6, due to pumping of Well INJ, are shown in Figure 2. This figure shows that there is a distinct difference between transmissivity data obtained from Wells 1 through 6. Hydrologists interpret these data to indicate that the transmissivity of the gravel formation is greatest in the west-east direction. Note that these curves represent a point measurement and are aliased in azimuth about the injection well so that they do not sample the bulk groundwater flow in all directions. Interpretation of groundwater flow patterns based on this limited amount of hydrological data is tenuous since significant stream channels may exist at azimuths not sampled by well data.

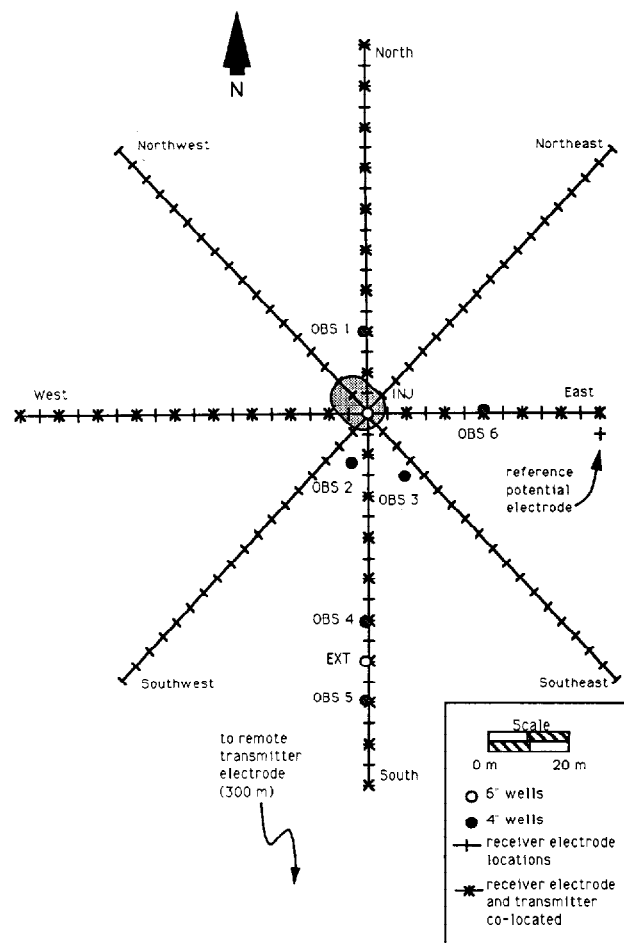


FIG. 1. This is a plan map of the well field and resistivity array at the Richmond Field Station. The shaded area in the center of the array represents the displacement of the injected salt water plume as inferred from the resistivity measurements. Potential measurement electrodes are located at 5-m intervals along the receiver lines. During the first injection experiment pole-pole measurements were made along the south-north and west-east receiver lines only. During the second experiment, pole-dipole measurements were made along the south-north, southwest-northeast, west-east, and northwest-southeast lines.

Salt water injection and extraction procedure

Salt water for the two injection experiments was obtained from San Francisco Bay and pumped into a holding pond 200 m south of the injection well. Salt and fresh water were pumped into the pond to adjust fluid conductivity. After mixing and settling to remove silt and mud, the water was passed through filters and pumped into the injection well. A total of 25 000 gallons of salt water was injected at an average flow rate of six gallons per minute for 72 hours. The conductivity of the native groundwater and the injected salt water were monitored throughout the experiment with a conductance meter. Conductivity probes were located in the injection well just above the screen and at the bottoms of the observation wells.

The conductivity of the native groundwater was measured to be 50 to 60 mS/m ($20 \Omega \cdot \text{m}$ to $17 \Omega \cdot \text{m}$) and the injected salt water was 1.3 S/m and 0.88 S/m ($0.76 \Omega \cdot \text{m}$ and $1.13 \Omega \cdot \text{m}$) for the first and second experiment, respectively. Since the injection zone is below the water table and the groundwater resistivity is known, the resistivity of the intruded formation can be estimated as

$$\rho_{\text{anomalous}} = \rho_{\text{formation}} * \left(\frac{\rho_{\text{salt water}}}{\rho_{\text{groundwater}}} \right)$$

For a groundwater resistivity of $17 \Omega \cdot \text{m}$ and a formation resistivity of $11 \Omega \cdot \text{m}$, the intruded zone would have a bulk resistivity of $0.5 \Omega \cdot \text{m}$ for the first experiment and $0.75 \Omega \cdot \text{m}$ for the second experiment. Since the intruded zone is more than ten times less resistive than the formation, electrical

saturation has occurred. The electrical contrast can therefore be considered to be the same for both experiments.

Assuming an aquifer thickness of 3 m and a porosity of 20 percent, it is easy to show that a 25 000 gallon injection would result in a cylindrical anomaly of 7 m radius under conditions of isotropic plug flow. No changes in groundwater conductivity were measured at the observation wells 15 m away.

Three days after injection was stopped, extraction was begun from the same well. The salt water was extracted at a rate of 20 gallons per minute for seven days until the outflowing fluid reached the same conductivity as the native groundwater. This resulted in a total extraction of 200 000 gallons, eight times the amount injected.

INSTRUMENTATION

During the first experiment resistivity measurements were made by injecting current at the surface electrodes and at the downhole metal segments of the casing and measuring potential along north-south and east-west profile lines that intersect at well INJ. All electrodes were wired into a position on the eastern end of the array and resistivity measurements were made from this one location. For the second experiment, more azimuthal information was obtained by adding receiver electrode lines between the north-south and east-west lines. These two experiments incorporated two different receiver electrode configurations. The first experiment was conducted with a pole-pole acquisition system and the second used a pole-dipole system.

The pole-pole configuration utilized a fixed reference transmitter electrode and a fixed reference receiver electrode. Measurements were made by energizing any one of 40 transmitter electrodes in concert with the reference transmitter electrode to obtain values of potential relative to the reference potential electrode at 76 surface and subsurface locations. The pole-dipole acquisition system utilized a fixed surface reference transmitter electrode and a set of 130 receiver dipoles. Measurements were made by energizing the borehole current electrodes in concert with the reference transmitter electrode and obtaining values of dipole voltage along eight radial lines on the surface of the earth. These lines radiate from the injection well and consist of up to 17 5-m measurement dipoles.

The receiver system is controlled by a microcomputer interfaced with a digital voltmeter. The electrode potentials are filtered and sampled sequentially. Timing for the sampling sequence and the transmitter is provided by a crystal clock. The transmitted waveform is a 10 A to 20 A square wave of frequency 0.1 Hz for the pole-dipole array and 0.2 Hz for the dipole-dipole array. This waveform is sampled over 30 cycles for each transmitter electrode location. This resulted in a total of 180 to 360 samples for each receiver electrode location.

Since temporal measurements are of concern, it is essential to insure that measurements taken on different days repeat when no geological or hydrological change has taken place, so numerous repeatability tests were performed. These tests showed that measurements repeated to within a couple of tenths of a percent over a period of several days to a week.

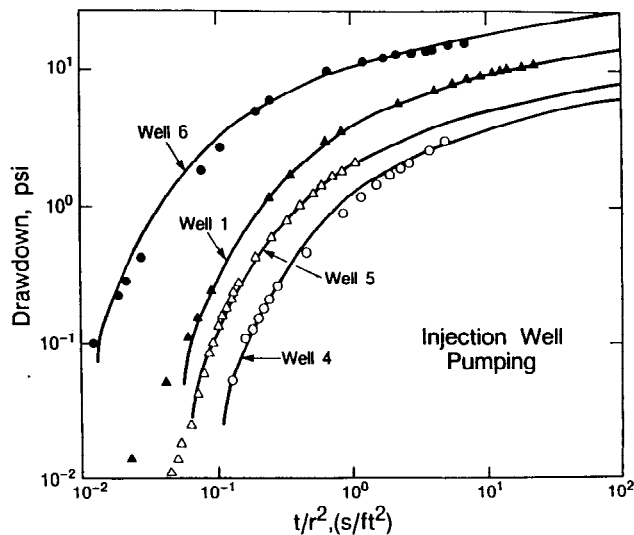


FIG. 2. These drawdown curves (from Javandel, 1988) represent the change in pressure (psi) as a function of time in each of the wells due to pumping of the injection well. This change in pressure is proportional to the change in water level in the wells. Since the observation wells are at various distances from the injection well, the time axis is normalized by distance squared (t/r^2). The drawdown in well 6 is greater than the drawdown in any of the other wells, indicating greater transmissivity between well 6 and the injection well than any of the other wells and the injection well.

ELECTRICAL RESISTIVITY MONITORING

For the first injection experiment, using the pole-pole array, a complete data set was taken before salt water injection, at maximum volume injected and after salt water extraction. A partial data set was collected every day with current sources at the 30 m and 40 m depths of the injection well. During the second experiment, using the pole-dipole array, data were taken by energizing transmitter electrodes at 30-m and 40-m depth in the injection well.

Throughout this paper the measurement results are presented as either apparent resistivity or normalized potential. The normalized potential is the observed voltage divided by the injected current.

Surface resistivity monitoring

Figure 3 is a surface dipole-dipole apparent resistivity pseudosection along the south-north line generated by superposing the pole-pole data. Apparent resistivities range from 10 to 25 $\Omega\cdot\text{m}$ within the pseudosection and increase with larger n -spacing or greater depth. The profile does not show any large lateral variations in resistivity although there are some indications of near-surface inhomogeneity.

The measurements were repeated after salt water was injected into the aquifer. The two data sets showed no significant change in apparent resistivity for low n -spacing and no significant effect on surface layer resistivity due to light rain. The main reason for this insensitivity to the salt injection is that a relatively small volume of rock is affected by the salt water compared to the volume of rock sampled by the measurements.

Borehole-to-surface resistivity monitoring

Since the zone of interest is at depth, the greatest change in the measurements is observed when the transmitter electrodes are located in the subsurface. To investigate the sensitivity of various arrays, the measured pole-pole potentials were superposed to create pole-dipole, dipole-dipole,

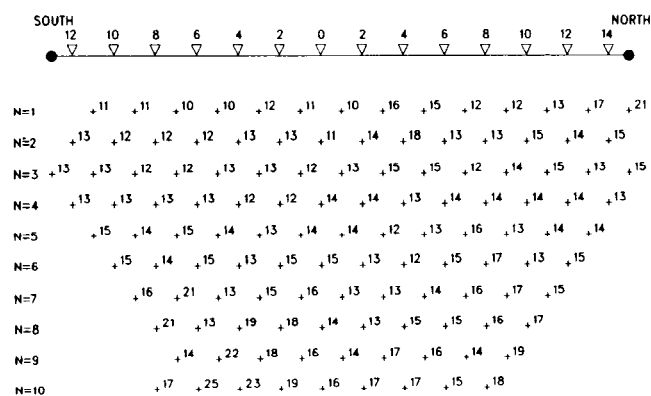


FIG. 3. The surface dipole-dipole pseudosection along the south-north line before salt water injection is shown here. The dipole length is 10 m and apparent resistivities are in $\Omega\cdot\text{m}$. The postinjection pseudosection showed no measurable change due to the injection and therefore is not displayed.

and dipole-pole potentials for apparent resistivity calculation.

The measured borehole-to-surface pole-pole potential before and after salt water injection is presented as Figures 4 and 5. The potential is negative for electrode locations beyond electrode number 12 because the reference electrode is located 60 m east and 10 m south of the center of the array. Since all potentials are measured relative to this reference electrode, they are positive for locations within about 60 m (around electrode number 12) of the center of the array, and negative for locations more than about 60 m from the center. On this scale it is difficult to see the effect of salt water injection. The data in Figure 4 are subtracted from the data in Figure 5 to create the time difference curves in Figure 6. These curves exhibit a strong asymmetric anomaly due to the presence of the salt water. However, the 1.5 mV/A anomaly represents only about 4 percent change over the

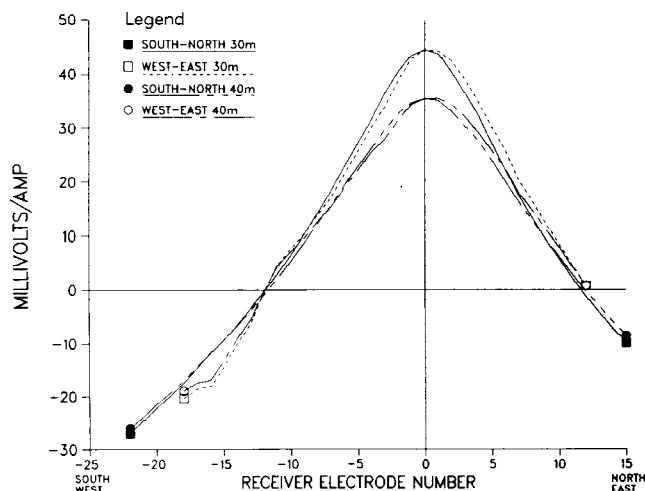


FIG. 4. Borehole-to-surface pole-pole potential before salt water injection. The potential was measured along the south-north and west-east lines with current sources at 30-m and 40-m depth in the injection well.

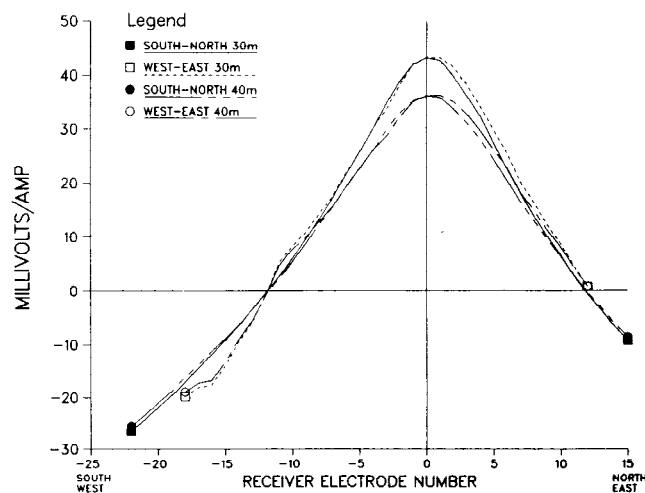


FIG. 5. Borehole-to-surface pole-pole potential at maximum salt water injection.

preinjection value. The anomaly is enhanced by subtracting the potential due to the source at 30 m depth from the potential due to the source at 40 m depth to simulate a dipole transmitter. This results in a smaller primary field, and a greater difference.

The result of this superposition is shown in Figures 7 and 8. Subtracting the preinjection potential from the postinjection potential results in the curves of potential difference shown in Figure 9. The maximum anomaly of about 2 mV/A represents a change of approximately 25 percent over the preinjection value. A notable feature of this data is the pronounced asymmetry of the curves.

In an attempt to further enhance the anomaly, the data were superimposed to simulate pole-dipole and dipole-dipole arrays. Although the pole-pole measurements have low standard deviation, the difference between potential at adjacent receiver electrode positions is also small. When these

small differences in potential are subtracted from one another to simulate dipole receivers the relevant measurement error increases unacceptably. This can be demonstrated by the following simple numerical example.

For the sake of discussion, assume a model with half-space resistivity $4\pi \Omega \cdot \text{m}$. The normalized voltage at a point on the surface directly above (at $x = 0 \text{ m}$) a transmitter electrode at 40-m depth is given by

$$\frac{V}{I} = \frac{\rho}{2\pi r} = \frac{2}{40} = 0.05 \text{ V/A},$$

similarly, at $x = 5 \text{ m}$ on the surface, the normalized voltage is 0.049613893 V/A. Subtracting these two pole voltages, the dipole voltage between a 0 m and 5 m receiver electrode is 0.38617 mV/A. If the pole voltages have a 0.1 percent error

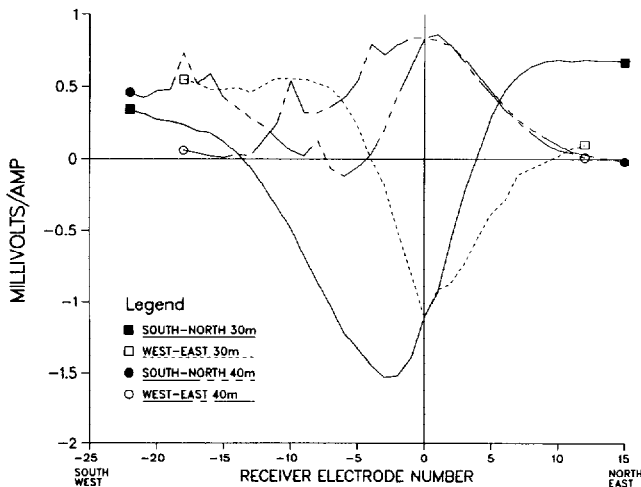


FIG. 6. Time difference of borehole-to-surface pole-pole potential. This is the result of subtracting the data in Figure 4 (preinjection) from the data in Figure 5 (postinjection).

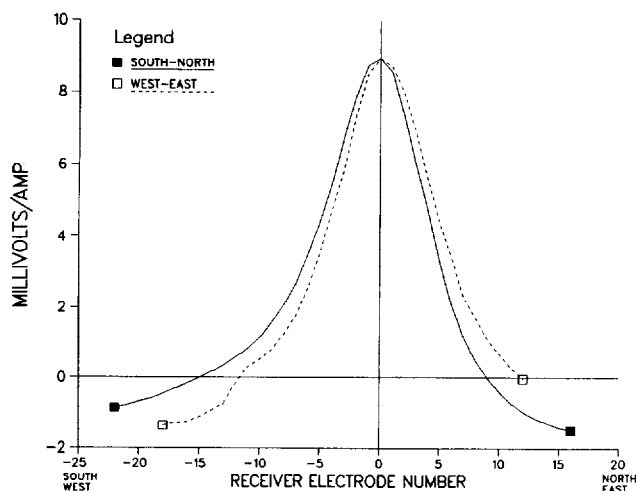


FIG. 7. Preinjection potential for the dipole-pole configuration. These curves were generated by superposition of the pole-pole measurements of Figure 4 into dipole-pole data.

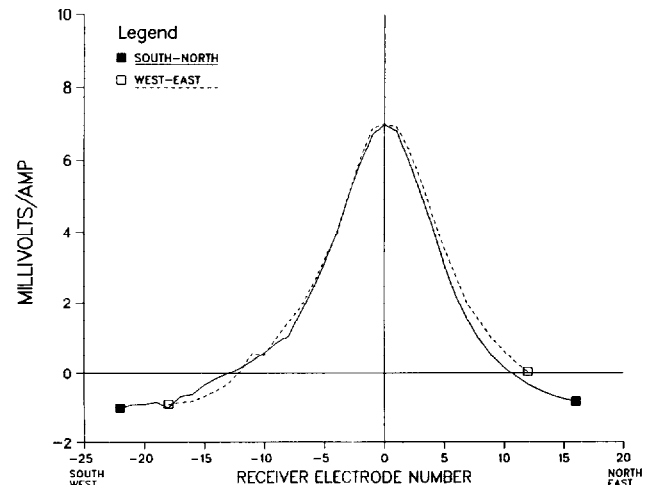


FIG. 8. Postinjection potential for the superposed dipole-pole configuration. These curves were generated by superposition of the pole-pole measurements of Figure 5 into dipole-pole data.

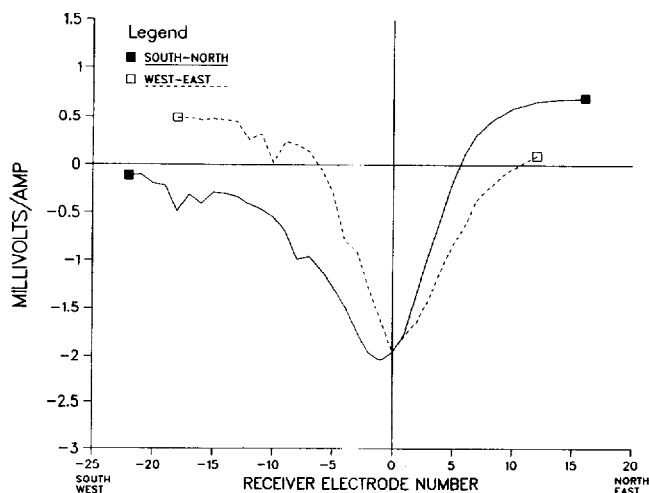


FIG. 9. Potential difference between preinjection and postinjection dipole-pole data. This is the result of subtracting the data of Figure 7 from the data of Figure 8.

(i.e., standard deviation of 0.05 mV/A), this is a 12.9 percent error for the dipole voltage. For a transmitter at 30-m depth, the normalized voltage at $x = 0$ m is 0.0666 V/A. This can be combined with the voltage due to the 40-m transmitter to get a dipole-pole normalized voltage of 0.01666 V/A. For this configuration, a pole-pole error of 0.1 percent translates into a dipole-pole error of 0.3 percent. From these numerical examples, it is evident that the superposition of pole-pole data to create surface dipoles leads to unacceptable error propagation, while superposition of the data to create sub-surface dipole transmitters remains within acceptable error tolerances.

The dipole-pole data are plotted as percent difference in Figure 10. Percent difference is defined as

$$\frac{(P_{\text{postinjection}} - P_{\text{preinjection}})}{P_{\text{preinjection}}} * 100.$$

Although the percent difference plot of the dipole-pole data (Figure 10) shows a distinct asymmetric anomaly, the potential difference plot (Figure 9) shows a sharper anomaly with more distinct features. The potential difference curves develop distinct positive lobes at distant electrode locations and sharp peak amplitudes near the array center.

Interpretation of dipole-pole potential data

The 3-D finite difference program developed by Dey and Morrison (1979) was used to model the effects of the conductive salt water slug. Computer memory limitations constrained the finite difference mesh size to 55 by 16 by 20 nodes on the IBM 3090. Figure 11 is a schematic diagram of the model half-space with a salt water block in place.

Figures 12 and 13 are plots of calculated borehole-to-surface dipole-pole potential difference due to a dipole transmitter with electrodes at 30-m and 40-m depth. The salt water target is progressively offset to the right in models 2 through 4 (Figure 14).

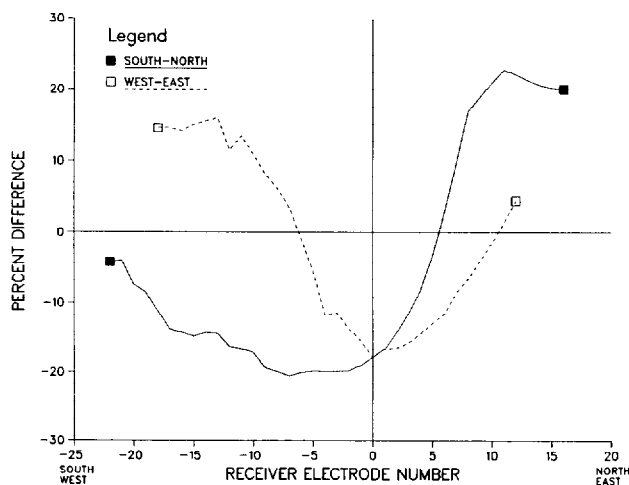


FIG. 10. Percent difference between preinjection and postinjection dipole-pole data. This is the result of taking the percent difference of the data in Figure 8 relative to the data of Figure 7.

Comparing the model results gives an indication of the sensitivity of these types of measurements to the size and relative position of the anomalous body. The results in Figure 12 are due to 2-m thick blocks. The volume of these blocks corresponds to an intruded zone of about 30-percent porosity. The results in Figure 13 are due to 3-m thick blocks corresponding to a porosity of about 20 percent. Asymmetric current channeling causes the potential in the direction of block displacement to fall off more slowly, so that the difference curves have a positive lobe in that direction. These curves represent an anomaly of 25- to 30-percent difference relative to the preinjection potential; this compares to a less than 1 percent difference for surface dipole-dipole results calculated for the same model (dipole separation of up to ten dipole lengths).

The finite difference mesh size restricts the variation of target shape and size. Also, the mesh size in the Y dimension is so limited that the body cannot be displaced in that

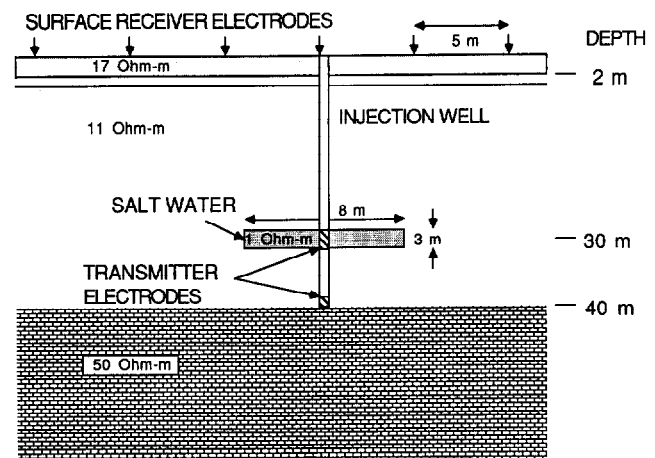


FIG. 11. Cross-section of the three-dimensional model used to simulate the salt water injection experiment.

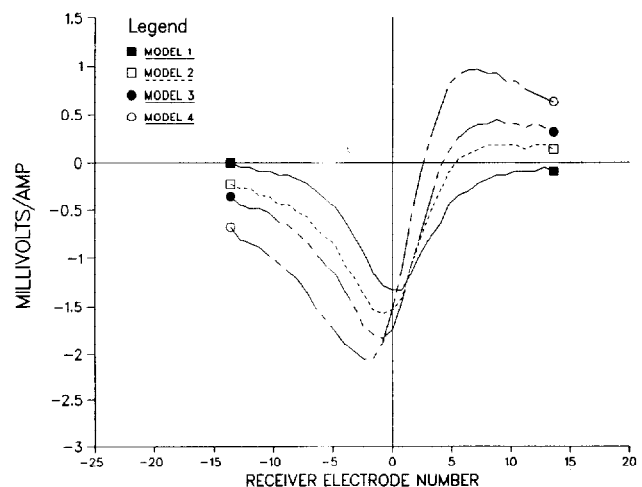


FIG. 12. Three-dimensional model results for the borehole-to-surface dipole-pole configuration. These curves of potential difference are for 2-m thick salt water block models corresponding to 30-percent formation porosity.

direction. Since run time for these models is about 20 minutes, successive forward modeling or data inversion is impractical and prohibitively expensive. With these modeling constraints, the best interpretation that can be achieved is to fit the model results to the observed data on a line by line basis as if the body were offset in only one direction. In this way it is possible to get a size and position sensitive match to the observed data.

The model curves have a positive lobe on the side corresponding to the direction in which the body is offset. The position of the curves minima and its amplitude also changes as the body is moved off-center. Comparing the south-north

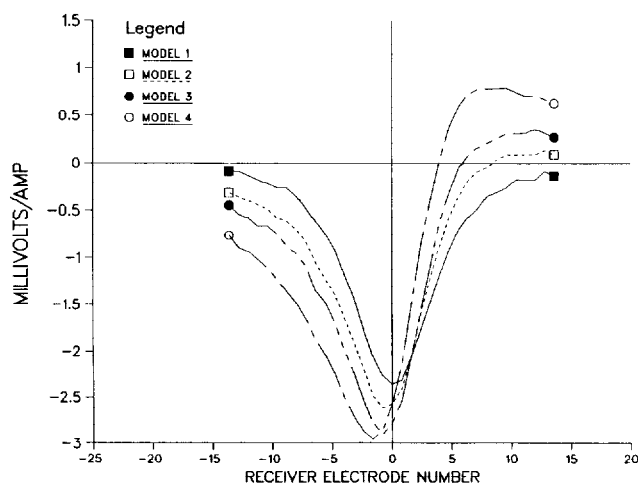


FIG. 13. Three-dimensional model results for the borehole-to-surface dipole-pole configuration. These curves of potential difference are for 3-m thick salt water block models corresponding to 20-percent formation porosity.

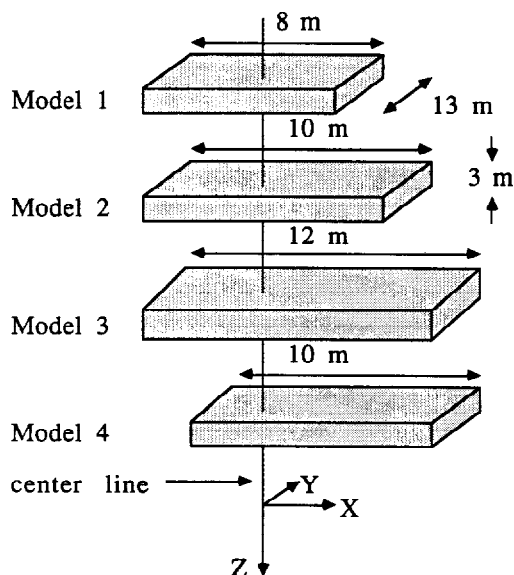


FIG. 14. Relative positions and dimensions of the salt water block models. All models are 3 m in the z direction, 13 m in the y direction, and from 8 to 12 m in the x direction.

difference data (Figure 9) to the model curves indicates a fit falling between the Figure 12 and 13 curves and matching the displacement of model 3. This corresponds to a displacement of the body to the north and a block size corresponding to 20 to 30 percent porosity. The character of the west-east data indicates a displacement to the west consistent with model 2. Therefore, the resistivity data indicates that the plume is displaced to the northwest, and the bulk transmissivity is greatest in this direction. This differs from the conclusion derived from the drawdown test (Figure 2), which indicates that the maximum transmissivity is to the east.

This is an example where resistivity measurement has an advantage over a limited number of hydrological measurements. The resistivity data are bulk measurements of an earth property that is affected by the overall resistivity distribution in the subsurface. It is therefore sensitive to plume displacement in any direction. The hydrological measurement is only sensitive to groundwater flow at the measurement point. Since there are no wells to the northwest of the injection well, the flow parameters cannot be sampled in that direction. The resistivity measurement allows the flow to be detected without the expense of drilling a series of densely spaced wells.

Dipole-dipole resistivity monitoring

The second injection experiment was done to confirm that the bulk formation transmissivity was greatest to the northwest by adding two new lines of receiver electrodes at 45 degrees to the south-north and west-east lines.

Although analysis of the first data set suggested that superposing pole-pole data to form dipole-pole data was best, the second set was gathered as pole-dipole and transformed into dipole-dipole. This was done for two reasons: (1) The signal levels and standard deviations of the pole-pole data are such that the subsurface data cannot be superposed into pole-dipole or dipole-dipole without introducing an excessive error, and analyzing dipole potential may really be the preferred approach since some model studies show it to be more sensitive to changes than pole potential (Eloranta, 1985). (2) The pole-dipole configuration was chosen for convenience because it was desired to make the acquisition system more portable in order to conduct larger scale surveys. Measuring dipole potential reduces the dynamic range requirements of the digital voltmeter and minimizes electromagnetic coupling effects. Also, the logistic problem of locating a reference receiver electrode in a noise free and convenient location is eliminated.

As in the pole-pole case, the anomaly can be enhanced by superposing the pole-dipole data from the 30-m and 40-m transmitter electrodes to create dipole-dipole potential. This decreases the effective amplitude of the observed potential. Figure 15 is the difference between the postinjection and preinjection data. These curves are not as smooth as the dipole-pole curves because dipole measurements are proportional to electric field, and electric field is discontinuous at resistivity contrasts. These curves show a maximum anomaly of about 40 percent.

The dipole-dipole potential for the 20-percent porosity model series (Figure 16) can be used to interpret the curves of Figure 15. The results in Figure 16 are for a series of

blocks displaced to the left. The dipole-dipole models are otherwise identical to the dipole-pole models in Figure 14.

There are several salient features to these model curves. The amplitude of the anomaly increases on the side corresponding to the direction of block displacement and the zero crossing shifts away from the direction of displacement. Also, the curves for the displaced blocks intersect the curve for the centered block. This intersection occurs at a lower receiver number for greater block displacement.

Analyzing the data of Figure 15 in light of these model results confirms the conclusion that the direction of maximum transmissivity is northwest. The amplitude of the northwest-southeast curve is maximum to the left, which is the northwest side of the line. The zero crossing is displaced to the southeast, indicating displacement to the northwest.

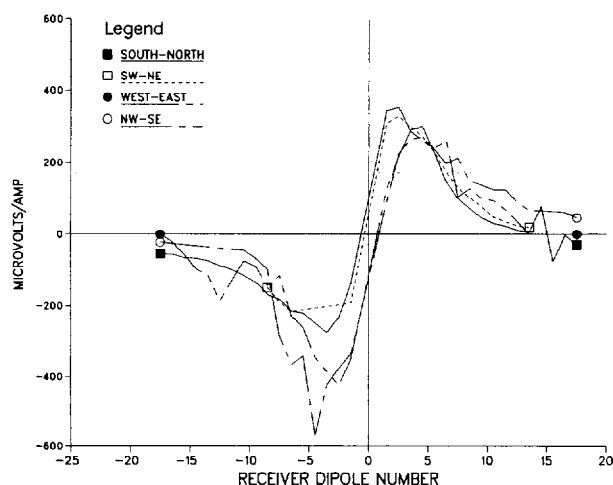


FIG. 15. Curves of difference relative to baseline for dipole-dipole data along the four receiver lines. These curves were generated by subtracting the preinjection data from the postinjection data.

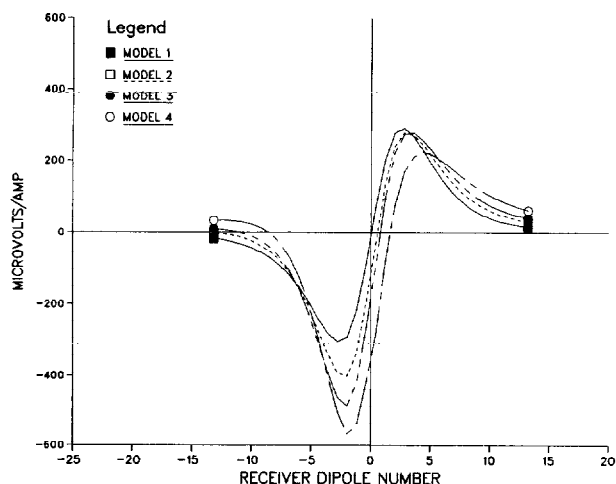


FIG. 16. Three-dimensional model results for the borehole-to-surface dipole-dipole configuration. These curves of potential difference are for 3-m thick salt water block models corresponding to 20-percent formation porosity.

For the other three lines, maximum displacements occur to the (in order of magnitude) west, north, and northeast. Since the northwest-southeast data shows the greatest amplitude, this must correspond to the direction of maximum bulk groundwater flow.

CONCLUSIONS

This experiment demonstrates that the borehole-to-surface electrical resistivity monitoring system is capable of gathering data accurately enough to map subsurface groundwater flow. The injected plume of salt water moves asymmetrically into the northwest quadrant from the injection hole. The pressure during drawdown tests indicates major transmissivity to the east although no test wells are available to measure transmissivity to the northwest. The resistivity results suggest strong channel flow paths that cannot be determined by a limited number of observation wells, but which are clear in the resistivity results.

The choice of how to present resistivity data is dependant on how the data are gathered. In this case, looking at time differences of potential, instead of apparent resistivity yields results that allow for easier interpretation.

The chief limitation to this method lies in the lack of adequate interpretive tools. The use of an integral equation solution or the development of an expanded mesh size and much faster run time would enable more detailed and accurate interpretation of field data. If the plume boundary could be accurately modeled, the size and position of the intruded zone could be better determined. This would allow the porosity and transmissivity of the aquifer to be estimated.

ACKNOWLEDGMENTS

The authors would like to thank Ted Asch, Alex Becker, Seunghye Lee, and Mike Wilt for their advice and efforts in this project. The comments of Craig Beasley and two anonymous reviewers are gratefully acknowledged.

Although the research described in this article has been supported by the United States Environmental Protection Agency through Agreement Number DW89932611 to Lawrence Berkeley Laboratory, it has not been subjected to Agency review and therefore does not necessarily reflect the views of the Agency and no official endorsement should be inferred. Mention of trade names or commercial products does not constitute endorsement or recommendation for use.

REFERENCES

- Asch, T., and Morrison, H. F., 1989, Mapping and monitoring electrical resistivity with surface and subsurface electrode arrays: *Geophysics*, **54**, 235-244.
- Beasley, C. W., and Ward, S. H., 1986, Three-dimensional mise-a-la-masse modeling applied to mapping fracture zones: *Geophysics*, **51**, 98-113.
- Daniels, J. J., 1977, Three-dimensional resistivity and induced polarization modeling using buried electrodes: *Geophysics*, **42**, 1006-1019.
- Daniels, J. J., 1983, Hole-to-surface resistivity measurements: *Geophysics*, **48**, 87-97.
- Dey, A., and Morrison, H. F., 1979, Resistivity modeling for arbitrarily shaped three-dimensional structures: *Geophysics*, **44**, 753-780.
- Eloranta, E. H., 1985, A comparison between mise-a-la-masse anomalies obtained by pole-pole and pole-dipole electrode configurations: *Geosplor.*, **23**, 471-481.

- Javandel, I., 1988, Personal communication. Earth Sciences Division, Lawrence Berkeley Laboratory, University of California, Berkeley, CA 94720.
- Le Masne, D., and Poirmeur, C., 1988, Three-dimensional model results for an electrical hole-to-surface method: Application to the interpretation of a field survey: *Geophysics*, **53**, 85–103.
- Poirmeur, C., and Vasseur, G., 1988, Three-dimensional modeling of a hole-to-hole electrical method: Application to the interpretation of a field survey: *Geophysics*, **53**, 402–414.
- Rodriguez, E. B., 1984, Ground water contamination studies in Ontario: NWWA/EPA Conf. on surface and borehole geophysical methods in ground water investigations, Feb. 1984, 603–617.
- Saunders, W. R., and Stanford, J. A., 1984, Integration of individual geophysical techniques as a means to characterize an abandoned hazardous waste site: NWWA/EPA Conf. on surface and borehole geophysical methods in ground water investigations, Feb. 1984, 584–602.
- Van Overmeeren, R. A., 1989, Aquifer boundaries explored by geoelectrical measurements in the coastal plain of Yemen: A case of equivalence: *Geophysics*, **54**, 38–48.
- Wilt, M. J., Pruess, K., Bodvarsson, G. S., and Goldstein, N. E., 1983, Geothermal injection monitoring with dc resistivity methods: *Geoth. Res. Council, Trans.*, Oct. 1983, 477–482.
- Wilt, M. J., and Tsang, C. F., 1985, Monitoring of subsurface contaminants with borehole/surface resistivity measurements: Lawrence Berkeley Laboratory Rep. no. LBL-19106.
- White, P. A., 1988, Measurement of ground water parameters using salt water injection and surface resistivity: *Ground water*, **26**, 179–186.
- Yang, F. W., and Ward, S. H., 1985a, Single-borehole and cross-borehole resistivity anomalies of thin ellipsoids and spheroids: *Geophysics*, **50**, 637–655.
- Yang, F. W., and Ward, S. H., 1985b, On sensitivity of surface-to-borehole resistivity measurements to the attitude and the depth to center of a three-dimensional spheroid: *Geophysics*, **51**, 1978–1991.